ChemPubSoc Europe

DOI: 10.1002/open.201402163

Open Access ChemistryOPEN Full Papers

Surfactant-Free and Controlled Synthesis of Hexagonal $CeVO_4$ Nanoplates: Photocatalytic Activity and Superhydrophobic Property

Xiaojuan Yang, Wenli Zuo, Feng Li, and Taohai Li*[a]

Nanomaterials with both superhydrophobic surface properties as well as photocatalytic activities could have important industrial applications. Herein, we synthesized $CeVO_4$ nanocrystals with hexagonal nanoplate structures from the reaction of decavanadate ($K_6V_{10}O_{28}{\cdot}9H_2O$) and $CeCl_3{\cdot}H_2O$ precursors via a hydrothermal method. This synthetic route has four advantages: 1) the reaction condition is relatively mild, 2) it doesn't need surfactants or templates, 3) it requires no expensive equipment, and 4) products are of higher purity. During synthesis, solution pH, and reaction temperature were found to play important roles in determining the growth process and final morphologies of the $CeVO_4$ products. These products were characterized spectrophotometrically and via scanning and transmission electron microscopy. Furthermore, the wettability of the as-synthesized film $CeVO_4$ nanoplates was studied by measuring water contact angle (CA). The largest CA measured was at 169.5° for a glass substrate treated with 0.06 g mL^{-1} $CeVO_4$ followed by 2% 1H, 1H, 2H, 2H-perfluorodecyltriethoxysilane. Finally, the $CeVO_4$ nanoplates exhibited excellent photocatalytic activity in degradation of rhodamine B (RhB) under UV irradiation and was stable even after repeated cycles of use.

Introduction

Nanomaterials are of great interest due to their potential applications in catalysis and optoelectronic devices, as well as their unique properties e.g. magnetic properties associated with their smaller dimensions.[1–6] Ternary system $CeVO_4$ shows high-activity catalysis in the oxidative dehydrogenation of propane at low temperature,[7] and it also represents a new class of optically inactive materials used as counter electrodes.[8] However, there are no reports about the superhydrophobicity of $CeVO_4$ nanocrystals.

Nowadays, the wetting properties of superhydrophobic surfaces have become attractive to various research groups. A water drop on such surfaces forms a nearly perfect sphere. In nature, many surfaces such as various plant leaves[9–14] exhibit amazing superhydrophobicity. We know that the ability of the nanostructured surface of the lotus leaf to repel water has become a symbol for the environment-friendly qualities of nanotechnology.[15] Superhydrophobic materials hold considerable promise with potential applications e.g. self-cleaning surfaces.

The wetting behavior of $CeVO_4$ nanocrystals with hexagonal nanoplate structures has not been reported to date. The conventional methods for the preparation of $CeVO_4$ include solid-state reactions,[16] microwave irradiation,[17] and the sol-gel[18] method. However, these could be disadvantageous as only small particles are usually formed by these methods. Thus, it is important to develop a low cost and convenient method for the synthesis of $CeVO_4$ nanocrystals with controlled, well-defined sizes and shapes. [19] The hydrothermal method was considered as one of the most promising solution-chemical methods for the controlled synthesis of $CeVO_4$ nanocrystals with well-controlled morphology,[20–26] crystal growth orientation, and structural properties. To the best of our knowledge, there have been no reports on the fabrication of $CeVO_4$ by hydrothermal methods using the novel precursor decavanadate.

Herein, we synthesized $CeVO_4$ nanocrystals with hexagonal nanoplate structures from the reaction of $K_6V_{10}O_{28}{\cdot}9H_2O$ and $CeCl_3{\cdot}H_2O$ precursors via a hydrothermal method. This synthetic route has four advantages: 1) the reaction condition is relatively mild; 2) it doesn't need surfactants or templates; 3) it requires no expensive equipment; 4) products are of higher purity. Therefore, it can provide a general method for other functional orthovanadate materials. Notably, we have adopted a novel vanadium source (isopolyanions) in the synthesis of $CeVO_4$. In aqueous solutions, isopolyanions have versatile structures. By controlling the pH value, the structure of isopolyanions can be controlled. This means that we can obtain isopolyanions with target structures by simply adjusting the pH to a certain value, which is important for the preparation of specific structures involving the Ce–V–O system. Rhodamine B (RhB) was chosen as a model pollutant to evaluate the photocatalytic activity of the nanoplates in aqueous medium under UV irradiation. The results showed that $CeVO_4$ degrades RhB

[a] X. Yang, W. Zuo, Dr. F. Li, Dr. T. Li
College of Chemistry, Key Lab of Environment Friendly Chemistry and Application of the Ministry of Education, Xiangtan University, Xiangtan 411105 (P. R. China)
E-mail: hnlth@xtu.edu.cn

under UV irradiation with excellent efficiency. In addition, water contact angle measurements suggested that $CeVO_4$ nanoplates have superhydrophobic properties; a static contact angle for water of over 150° was observed.

Results and Discussion

Characterization of hexagonal $CeVO_4$ nanoplates

Figure 1 A shows the X-ray diffraction (XRD) patterns of the products obtained via hydrothermal method at different pH

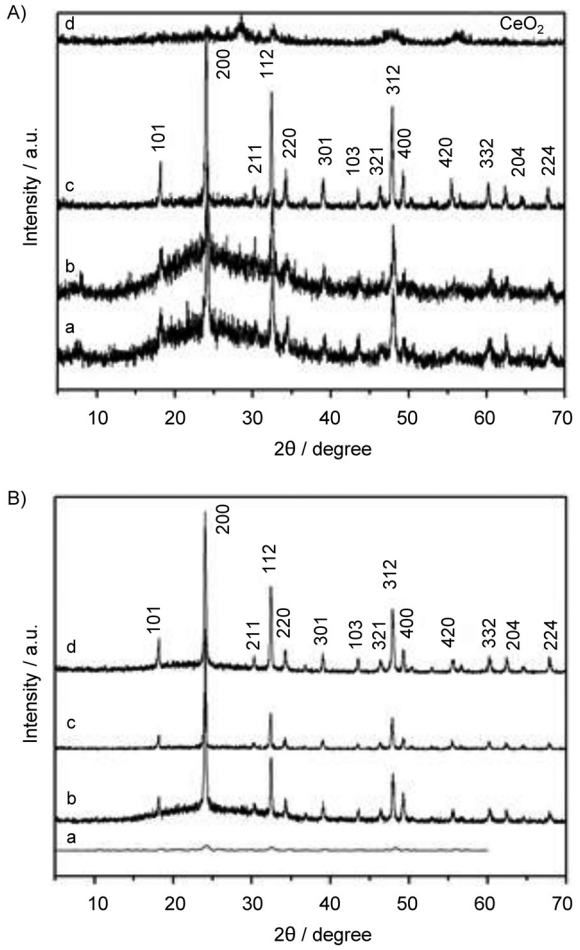

Figure 1. X-ray diffraction patterns of $CeVO_4$ nanocrystals obtained A) at 140 °C, with varying pH: pH 5 (a), pH 7 (b), pH 9 (c), and pH 11 (d) and B) at pH 9, with varying reaction temperatures: rt (a), 120 °C (b), 140 °C (c), and 160 °C (d).

values. The products synthesized at pH values of 5, 7, and 9 show similar patterns, which can be indexed as the tetragonal zircon phase of $CeVO_4$ (space group: *I41/amd*) with cell constants $a = b = 7.399$ Å and $c = 6.496$ Å, which are in good agreement with the standard values for the tetragonal phase $CeVO_4$ (Joint Committee on Powder Diffraction Standards (JCPDS) No. 12-0757). However, the peaks for CeO_2 were also observed at pH 11. All peaks of the product are broadened because of the small size of the crystals. Obviously, the pH of the solution plays an important role in the preparation of pure $CeVO_4$ via hydrothermal method, indicating the existence of somewhat preferential orientations in the $CeVO_4$ nanocrystals. From Figure 1 A, we can observe that the crystallinity of the product is optimal at pH 9.

To investigate the effect of temperature on the crystallinity, we also prepared $CeVO_4$ at different temperatures. The XRD patterns of the products can be seen in Figure 1 B. At room temperature, the crystallinity of as-prepared product is considerably low, and the uniformity is not perfect. Only a few peaks can be observed. However, a higher temperature supports the formation of the thermodynamically stable, well-crystallized, and uniform products. It is very clear that the crystallinity of obtained products increases with increasing reaction temperature at a fixed solution pH, as shown in Figure 1 B. Thus, the temperature of reaction systems also plays an important role in $CeVO_4$ crystal formation.

To further confirm the formation of the $CeVO_4$ crystal structure, Fourier transform infrared (FT-IR) spectroscopy was performed on the as-prepared $CeVO_4$ nanocrystals, as shown in Figure 2. A strong absorption band at 814 cm^{-1} and a weak

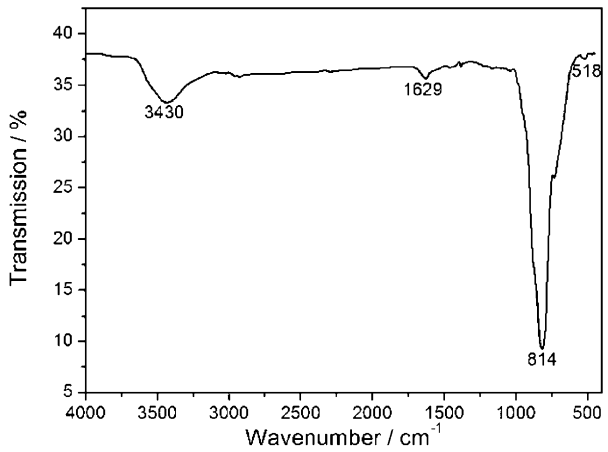

Figure 2. The FT-IR spectrum of $CeVO_4$ nanocrystals synthesized at 140 °C and pH 9.

band at 518 cm^{-1} can be attributed to the adsorption of V–O (from the VO_4^{3-} group) and Ce–O bond, respectively,[28] which implies that the crystalline $CeVO_4$ phase has formed in the as-prepared product. The absorption bands located at 3430 cm^{-1} and 1629 cm^{-1} can be ascribed to the O–H stretching and bending vibration of water. Because the product was prepared in aqueous solution, its surface can be inevitably covered with absorbed water molecules.

Analysis of morphology

Figure 3 A, a typical scanning electron microscopy (SEM) image of the $CeVO_4$ nanocrystals synthesized at 120 °C and pH 8, shows that the obtained products resemble hexagonal particles. It is also interesting that at pH 9, the products mainly consist of hexagonal and a few peach-like plates, as shown in Fig-

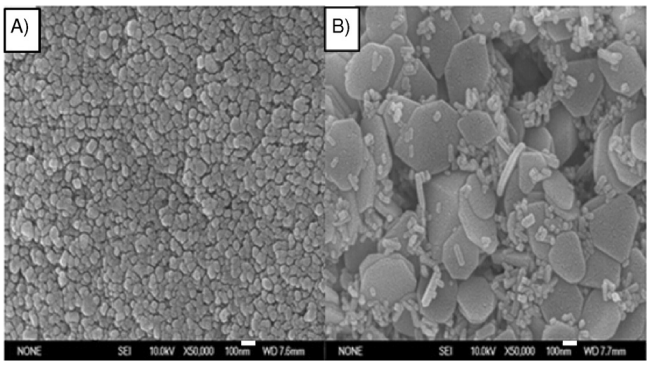

Figure 3. SEM images of $CeVO_4$ nanocrystals synthesized at 120 °C at pH 8 (A) and pH 9 (B). The white scale bars represent 100 nm.

ure 3B. Besides these, small rod-like particles with nonhomogeneous size distribution can also be observed. These results indicate that pH is a key factor in the formation of hexagonal nanoplates.

The typical and high-resolution transmission electron microscopy (HRTEM) images of the $CeVO_4$ nanocrystals synthesized at pH 9, with different reaction temperatures is illustrated in Figure 4. Figure 4A shows that when the reaction temperature was 120 °C, the obtained products were rod-like particles as well as some irregular shaped plates. When the reaction temperature was increased to 140 °C, hexagonal nanoplate structures of $CeVO_4$ could be obtained, with improved aspect ratio, and the rod-like particles disappeared (Figure 4B). Aside from this, a few peach-like plates which have not changed into hexagonal nanoplates could also be observed. The high-resolution TEM image of a single hexagonal nanoplate (Figure 4C) shows that the plate was well-crystallized with the (200) fringes running along the plate direction and spaced by 0.37 nm. The (101) fringes could also be observed with a spacing of 0.49 nm, which is consistent with growth of the plate along the [001] direction. The corresponding selected area electron diffraction (SAED) pattern (inset of Figure 4B) also indicates that the plates were well crystallized. Increasing the reaction temperature to 160 °C yielded irregular-shaped plates, as shown in Figure 4D. Over-all, we can conclude that temperature is also a critical factor which can affect the morphologies of $CeVO_4$ nanocrystals.

In order to better understand the formation and evolution of $CeVO_4$ nanostructures at 140 °C, the product morphology at this temperature but different pH values was explored. The TEM image of the product obtained at pH 8 is shown in Figure 5A. It is clearly seen that the product is composed of rod-like particles with nonhomogeneous size distribution, accompanied by the appearance of irregular-shaped plates. When the pH was adjusted to 9, hexagonal nanoplates were formed,

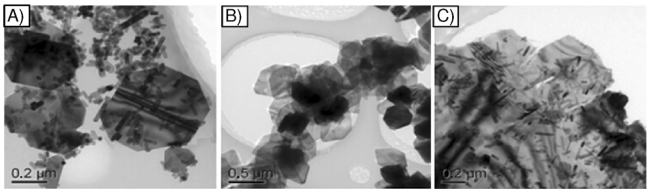

Figure 5. TEM images of the $CeVO_4$ nanocrystals synthesized under 140 °C at pH 8 (A), pH 9 (B), and pH 10 (C). The scale bars represent 0.2 μm, 0.5 μm, and 0.2 μm, for (A), (B), and (C), respectively.

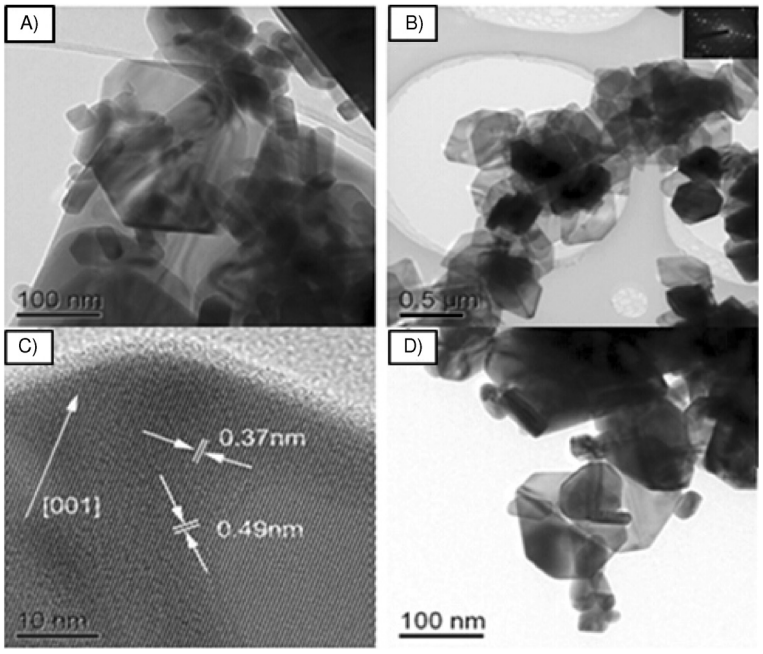

Figure 4. TEM and HRTEM images of the $CeVO_4$ nanocrystals synthesized at pH 9 and 120 °C (A), 140 °C (B) or 160 °C (D). The small inset of (B) shows the selected area electron diffraction (SAED) pattern. (C) shows the HRTEM image of a single hexagonal nanoplate of (B).

and rod-like particles disappeared (Figure 5B). At pH 10, abundant rod-like particles appeared with lengths of about 20 nm. These were different from those observed at pH 8, as these rod-like particles were longer and thinner than the morphology at the lower pH (Figure 5C).

Mechanism for the formation of $CeVO_4$ nanoplates

It is believed that the growth of the hexagonal nanoplate structure of $CeVO_4$ was not catalyst assisted nor template directed, because no additional surfactants nor templates were introduced in the reaction. The formation of $CeVO_4$ hexagonal nanoplates could be explained as follows: First, small hexagon-like particles dissolved, and components deposited on larger particles, gradually forming rod-like particles with nonhomogeneous size distribution. With an increase in pH, these rod-like structures grew into irregular-shaped plates including the observed peach-like plates (Figure 5A). After this, the peach-like plates translated into hexagonal nanoplates along the *c*-crystal axis. Upon a further increase to pH 9, the products formed mainly consisted of hexagonal and

a few peach-like plates (Figure 5B). Finally, at pH 10, the obtained products became rod-like particles with lower aspect ratios (Figure 5c).

Tha morphology analysis shows that the hexagonal structure of $CeVO_4$ obtained via our approach is mainly due to the effect of pH. When the reaction temperature was 120 °C or 140 °C, hexagonal nanoplates were formed at pH 9. However, when the pH was 8 or 10, this was not the main morphology. Thus, the presence of sodium hydroxide in this system could change the behavior of crystallization and growth orientation in a way that affects the product morphology. We also concluded that extending the reaction temperature would mainly prolong the rounds of formation along a specific direction forming the hexagonal nanoplates.

In order to understand the formation process of $CeVO_4$ hexagonal nanoplates at pH 9, SEM images of products obtained at different reaction times were taken (Figure 6). For a reaction

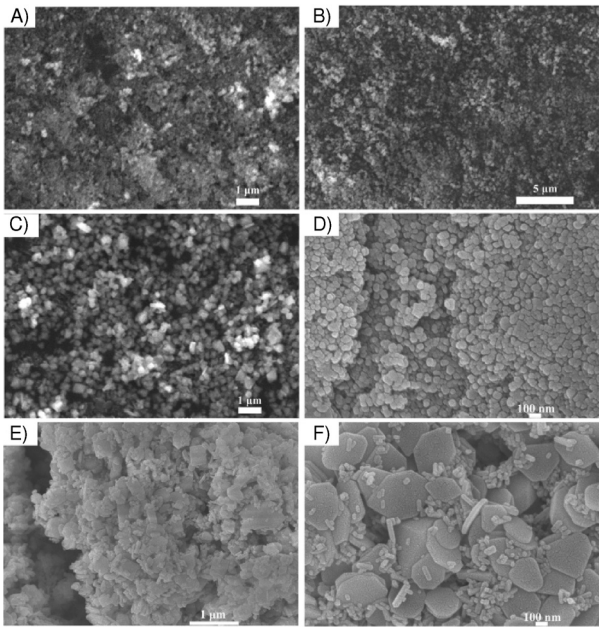

Figure 6. SEM images of CeVO4 hexagonal nanoplates obtained at different reaction times : 0 h (A), 6 h (B), 12 h (C), 24 h (D), 36 h (E), and 48 h (F). White scale bars for (A)—(F) represent 1 μm, 5 μm, 1 μm, 100 nm, 1 μm, and 100 nm, respectively.

time of 0 h, the product was composed of irregular nanoparticles. As the reaction time was extended to 6 h, the nanoparticles became larger, to a length of about 10 nm. After 12 h hydrothermal reaction, homogeneous and monodispersed nanoparticles were also obtained. At 24 h, the nanoparticles were transformed into nanoplates with a circular morphology. Upon further prolonging the reaction time to 36 h, the products became irregular aggregations of nanoplates, and abundant short rod-like particles were formed. After 48 h, a great deal of uniform hexagonal nanoplates and some rod-like particles were formed. Therefore, as the reaction time increases, the crystals grow and eventually form hexagonal nanoplates.

UV/Vis spectroscopy of $CeVO_4$ nanocrystals

UV/Vis spectroscopy was used to characterize the optical properties of the $CeVO_4$ nanocrystals as shown in Figure 7. Samples for these experiments were prepared by dispersing the as-prepared products in ethanol followed by sonication for 30 min to form clear solutions. All of these solutions showed a broad absorption peak at about 280 nm, no matter what kind of synthetic method or reaction precursors we used, which could be attributed to the VO_4^{3-} group existing in a nanocrystalline lattice.

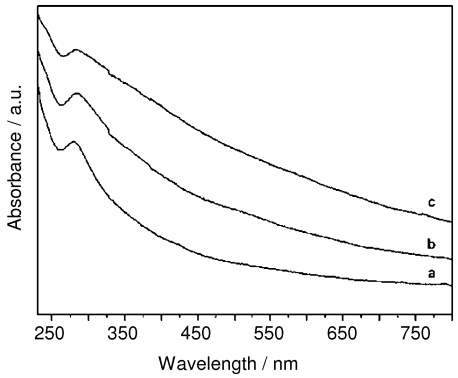

Figure 7. UV/Vis spectra of as-synthesized $CeVO_4$ nanocrystals at pH 9, and different reaction temperatures: 120 °C (a), 140 °C (b), 160 °C (c).

Photocatalytic performance

The temporal evolution of the spectral changes taking place at 554 nm during the photodegradation of RhB over $CeVO_4$ is shown in Figure 8A. The color of the suspension changed from pink to colorless. The as-prepared nanocatalysts exhibited excellent photocatalytic activity for the photodegradation of RhB under UV irradiation (94.8% degradation in 40 min). For comparison, we evaluated RhB degradation with photocatalysts in the dark and also in the absence of catalysts (i.e. direct photolysis) (Figure 8B). These tests confirmed that RhB did not degrade in the dark nor in the absence of photocatalysts under UV irradiation. Thus, we can be sure that the photocatalytic effect of $CeVO_4$ is responsible for the degradation of RhB, and that it is not due to direct photolysis of the dye nor mere adsorption on the photocatalysts. The active site appears to be V^{5+}–O–Ce^{3+} for the systems. The redox cycle for oxidative dehydrogenation appears to be associated with Ce-mediated redox reactions that lead to C–C bond breakage.

To observe photocatalyst stability after repeated use, we conducted recycling experiments. As shown in Figure 9, the RhB photodegradation efficiency of the catalyst decreases to just 90% from 94.8% after four runs of 40 min each. This indicates the nanocatalysts are still stable after repeated UV irradiation.

Adsorption and photocatalytic degradation are the two major processes of such a photocatalytic reaction. For the photocatalytic degradation process, active species play a major role. The hydroxyl radical ($OH^{\bullet}$) and proton (H^+) are the main active species for the degradation of dye molecules. Therefore

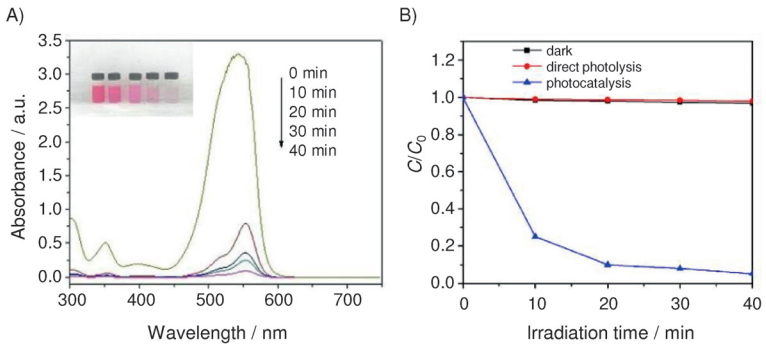

Figure 8. A) UV/Vis absorption spectral changes of RhB under the photocatalytic degradation process. B) Kinetics of degradation of RhB under different conditions.

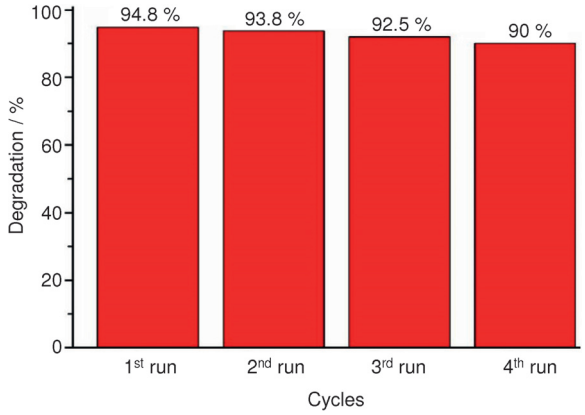

Figure 9. Repeated cycles of UV-induced photocatalytic degradation of RhB using the $CeVO_4$ photocatalyst.

a variety of radical scavengers, namely *tert*-butanol (*t*-BuOH), potassium iodide, and silver nitrate, were applied to the process of RhB degradation in the presence of the as-prepared nanocatalysts. *t*-BuOH is a well-known hydroxyl radical scavenger. As shown in Figure 10, the photodegradation rate was almost not changed when *t*-BuOH (10 mmol L^{-1}) was added, implying that the hydroxyl radical does not play a major role in the degradation of RhB. It is well known that potassium iodide is an effective H^+ scavenger. When potassium iodide (2 mmol L^{-1}) was added, the degradation of RhB was suppressed, indicating the participation of the H^+ in the photocatalytic reaction. On the other hand, this result was also confirmed by the improvement of the photocatalytic activity upon the addition of silver nitrate (an e^- scavenger), evidently due to the exposure of additional holes. Silver nitrate efficiency enhances the separation of photogenerated electrons and holes and lets more holes move to the surface of the catalyst. The above results demonstrate that H^+ is the main active species in the UV-induced photocatalytic reaction using the as-prepared nanocatalysts.

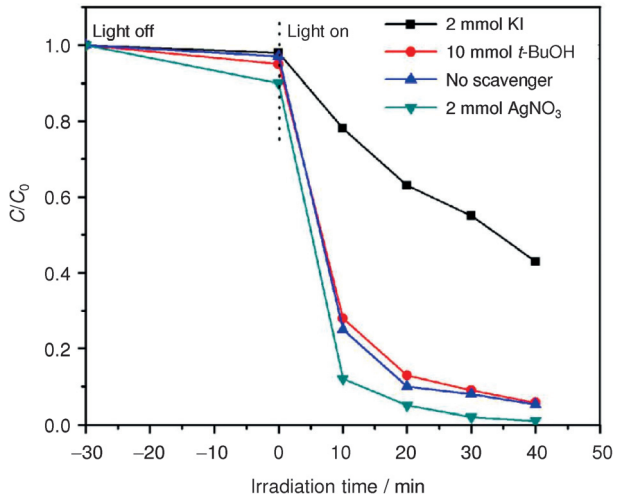

Figure 10. Time course of the UV-induced photodegradation of RhB using as-prepared nanocatalysts in the presence of various scavengers.

Contact angle (CA) measurements

Surface wettability of the as-synthesized hexagonal $CeVO_4$ nanoplates was studied by measurement of the water CA using a water droplet of 10 µL (Figure 11). Figure 11 A shows a CA value of 63.9° for the untreated glass surface. Figure 11 B shows a CA value of 92.9° after the glass surface was treated with a methanol solution of 2% (*v*/*v*) 1 H, 1 H, 2 H, 2 H-perfluorodecyltriethoxysilane (PFOTS) for 1 h at room temperature, followed by drying at 120 °C for 1 h. The CA values of the glass treated with as-synthesized $CeVO_4$ nanoplates were then measured. In the first step, the glass surface was modified by slow evaporation of a dilute ethanol dispersion of $CeVO_4$ nanoplates, followed by drying at 80 °C for 30 min. The $CeVO_4$ concentration was varied from 0.02, 0.04, and 0.06 g mL^{-1}. In a second step, a methanol solution of 2% PFOTS was added on the glass surface for 1 h at room temperature, followed by drying at 120 °C for 1 h. As shown in Figure 8 C–E, the CA values are 134.1° (Figure 11 C), 152.3° (Figure 11 D), and 169.5°

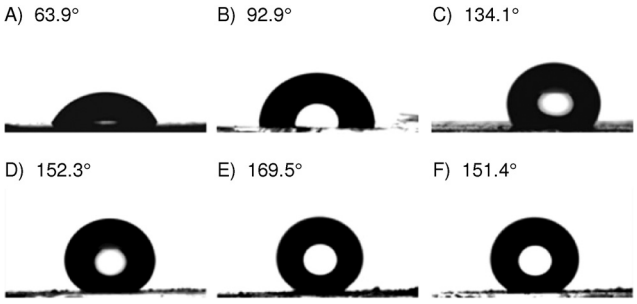

Figure 11. Water contact angle (CA) measurements of glass substrates without any treatment (A), with PFOTS (B), first treated with $CeVO_4$ at 0.02, 0.04, and 0.06 g mL^{-1}, then treated with 2% PFOTS (C—E, respectively), and with just $CeVO_4$ at 0.06 g mL^{-1}.

(Figure 11 E), corresponding to 0.02, 0.04, and 0.06 g mL^{-1} $CeVO_4$, respectively. Figure 8 F shows a CA value of 151.4° when the glass was only treated with a dilute ethanol solution of $CeVO_4$ nanoplates at 0.06 g mL^{-1}. From these results, we can see that the superhydrophobicity of the glass modified by the as-synthesized $CeVO_4$ nanoplates and PFOTS can be attributed to constructing a rougher texture on the glass surface and chemical treatment.

Conclusions

In summary, nearly monodisperse hexagonal $CeVO_4$ nanoparticles were synthesized under a hydrothermal method in pure water without surfactants. The $CeVO_4$ nanoplates show excellent photocatalytic activity in degrading RhB dye with nearly 94.8% degradation achieved in merely 40 min of UV irradiation. At the same time a contact angle of up to 169° could be achieved on a glass surface modified with 0.06 g mL^{-1} $CeVO_4$ followed by 2% 1H, 1H, 2H, 2H-perfluorodecyltriethoxysilane (PFOTS) in methanol. This work provides a new strategy to prepare novel multifunctional semiconductor $CeVO_4$ nanomaterials with potential industrial applications, such as self-cleaning materials, corrosion prevention, and environmental protection.

Experimental Section

Synthesis of $CeVO_4$ nanoplates

The decavanadate ($K_6V_{10}O_{28}\cdot 9H_2O$) was prepared according to a previously described procedure.[27] $CeVO_4$ nanocrystals were prepared by hydrothermal method in the absence of any organic additives. All reagents were of analytical grade and were purchased from Shanghai Chemical Co. Ltd. In a typical procedure, $CeCl_3\cdot 7H_2O$ powder (0.065 g) was dissolved in distilled H_2O (75 mL), stirred for 5 min at rt, then $K_6V_{10}O_{28}\cdot 9H_2O$ (0.103 g) was added while stirring. NaOH (2 M) was added dropwise to adjust the pH to the desired value (from 3 to 12). The resulting suspension was transferred into a 100 mL Teflon-lined stainless steel autoclave and sealed tightly. Hydrothermal synthesis was carried out at 120–160 °C for 48 h in an electric oven without shaking or stirring. After cooling to rt, the precipitates were collected, washed with distilled H_2O and absolute EtOH for several times, and then dried in a vacuum oven at about 60 °C for 10 h. The product was obtained in 69% yield.

Characterization

X-ray diffraction experiments were done on a MiniFlex II X-ray powder diffractometer (Rigaku, Tokyo, Japan) using Cu $K\alpha$ radiation ($\lambda = 0.15406$ nm). The TEM images were recorded on a JEOL JEM-2010 microscope (Tokyo, Japan) at an accelerating voltage of 200 kV. For TEM, the powder samples were ultrasonically dispersed in EtOH, and then deposited and dried on the holey carbon film on a copper grid. The SEM images were recorded on a JEOL JSM-6700F electron microscope. For spectrophotometric measurements, a Lambda 25 UV/Vis spectrophotometer and a NICOLET 380 FT-IR instrument from PerkinElmer were used (Waltham, USA). Water contact angle (CA) measurements were done on a water droplet (drop volume 10 μL) at rt using a Model 250 (p/n 250-F1) goniometer (Ramé-Hart Instrument Co., Succasunna, USA).

Measurement of photocatalytic properties

The photocatalytic activity of the $CeVO_4$ hexagonal nanoplates was evaluated by degradation of aqueous RhB under irradiation from a 300 W high-pressure mercury lamp. Photocatalyst (0.05 g) was added to the RhB solution (50 mL of 20 mg L^{-1}), and the dispersion was stirred for 30 min in the dark to achieve adsorption–desorption equilibrium prior to irradiation. After irradiation for 40 min, 5 mL of the solution was taken out and centrifuged to remove the catalysts. The UV/Vis absorption spectrum was then recorded on a Lambda 25 UV/Vis spectrophotometer.

Wettability measurement

The glass substrates were first ultrasonicated in acetone, EtOH, and ultrapure H_2O for 10 min each to get rid of surface contamination, and then dried in a vacuum oven at about 60 °C for 6 h. A specific amount of $CeVO_4$ was then added to 2 mL EtOH solution and ultrasonicated for 30 min. Then, five drops of suspension were dipped on the glass substrate to form a thin film, followed by drying at rt, then complete drying in the oven at 80 °C for 1 h. After that, the substrate was dipped in a 2% PFOTS solution at rt once for 30 min. Contact angle measurements were then carried out by using a contact angle meter (Ramé-Hart Instrument Co) at rt.

Acknowledgements

The authors acknowledge the financial support of the Provincial Natural Science Foundation of Hunan, China (13JJ6041, 2015JJ2138), and the National Natural Science Foundation of China (21343008).

Keywords: $CeVO_4$ · hexagonal · nanoplates · photocatalytic degradation · superhydrophobicity

[1] J. Hu, T. W. Odom, C. M. Lieber, *Acc. Chem. Res.* **1999**, *32*, 435–445.
[2] X. L. Hu, Y. J. Zhu, *Langmuir* **2004**, *20*, 1521–1523.
[3] H. Guan, C. Shao, B. Chen, J. Gong, X. Yang, *Inorg. Chem.* **2003**, *6*, 1409–1411.
[4] G. R. Patzke, F. Krumeich, R. Nesper, *Angew. Chem. Int. Ed.* **2002**, *41*, 2446–2461; *Angew. Chem.* **2002**, *114*, 2554–2571.
[5] R. Kalai Selvan, A. Gedanken, P. Anilkumar, *J. Cluster Sci.* **2009**, *20*, 291–305.
[6] G. H. Yue, P. X. Yan, D. Yan, J. Z. Liu, D. M. Qu, Q. Yang, *J. Cryst. Growth* **2006**, *293*, 428–432.
[7] Z. M. Fang, Q. Hong, Z. H. Zhou, S. J. Dai, W. Z. Weng, H. L. Wan, *Catal. Lett.* **1999**, *61*, 39–44.
[8] G. Picardi, F. Varsano, F. Decker, U. Opara-Krasovec, A. Surca, B. Orel, *Electrochim. Acta* **1999**, *44*, 3157–3164.
[9] W. Barthlott, C. Neinhuis, *Planta Med.* **1997**, *202*, 1–8.
[10] B. Bhushan, Y. C. Jung, *J. Phys. Condens. Matter* **2008**, *20*, 225010.
[11] W. Li, A. Amirfazli, *J. Colloid Interface Sci.* **2005**, *292*, 195–201.
[12] K. Koch, B. Bhushan, Y. C. Jung, W. Barthlott, *Soft Matter* **2009**, *5*, 1386–1393.
[13] W. Li, G. P. Fang, Y. F. Li, G. J. Qiao, *J. Phys. Chem. B* **2008**, *112*, 7234–7243.
[14] B. Bhushan, E. K. Her, *Langmuir* **2010**, *26*, 8207–8217.
[15] S. Herminghaus, *Europhys. Lett.* **2000**, *52*, 165.
[16] A. Watanabe, *J. Solid State Chem.* **2000**, *153*, 174–179.
[17] H. Wang, Y. Q. Meng, H. Yan, *Inorg. Chem. Commun.* **2004**, *7*, 553–555.
[18] U. Opara Krasovec, B. Orel, A. Surca, N. Bukovec, R. Reisfeld, *Solid State Ionics* **1999**, *118*, 195–214.
[19] L. Qian, J. Zhu, Z. Chen, Y. Gui, Q. Gong, Y. Ping, *Chem. Eur. J.* **2009**, *15*, 1233–1240.

[20] C. S. Shan, W. J. Zhao, Z. Cao, A. L. Elias, R. Cruz-Silva, M. Terrones, B. Wei, *Nano Lett.* **2013**, *13*, 5514 – 5520.
[21] C. T. Dinh, Y. Seo, T. D. Nguyen, F. Kleitz, *Angew. Chem.* **2012**, *51*, 6608 – 6612.
[22] T. D. Nguyen, D. Mrabet, C. T. Dinh, T. O. Do, *CrystEngComm* **2011**, *13*, 1450 – 1460.
[23] X. F. Duan, Y. Hang, R. Agarwal, C. M. Lieber, *Nature* **2003**, *421*, 241 – 245.
[24] F. Liu, X. Shao, Y. Yin, L. Zhao, Q. Sun, Z. Shao, X. Liu, *J. Rare Earth* **2011**, *29*, 97 – 100.
[25] W. Yu, G. Li, L. Zhou, *J. Rare Earth* **2010**, *28*, 171 – 175.
[26] B. M. Nath, A. Choudhury, A. Kundu, C. N. R. Rao, *Adv. Mater.* **2003**, *15*, 2098 – 2101.
[27] J. N. Xu, G. Y. Yang, H. R. Sun, T. G. Wang, *Hua Hsueh Yen Chiu Yu Ying Yung Chem. Res. Appl.* **1997**, *9*, 576 – 581.
[28] M. L. Pang, J. Lin, M. Yu, S. B. Wang, *J. Solid State Chem.* **2004**, *177*, 2237 – 2241.

Received: December 22, 2014
Published online on March 30, 2015

